JGP Journal of General Physiology

COMMUNICATION

Localized cardiomyocyte lipid accumulation is associated with slowed epicardial conduction in rats

Simon P. Wells[1,2], Antonia J.A. Raaijmakers[1], Claire L. Curl[1], Christopher O'Shea[2], Sarah Hayes[3], Kimberley M. Mellor[1,4,5], Jonathan M. Kalman[6,7], Paulus Kirchhof[2,8,9], Davor Pavlovic[2], Lea M.D. Delbridge[1*], and James R. Bell[1,3*]

Transmural action potential duration differences and transmural conduction gradients aid the synchronization of left ventricular repolarization, reducing vulnerability to transmural reentry and arrhythmias. A high-fat diet and the associated accumulation of pericardial adipose tissue are linked with conduction slowing and greater arrhythmia vulnerability. It is predicted that cardiac adiposity may more readily influence epicardial conduction (versus endocardial) and disrupt normal transmural activation/repolarization gradients. The aim of this investigation was to determine whether transmural conduction gradients are modified in a rat model of pericardial adiposity. Adult Sprague-Dawley rats were fed control/high-fat diets for 15 wk. Left ventricular 300 µm tangential slices were generated from the endocardium to the epicardium, and conduction was mapped using microelectrode arrays. Slices were then histologically processed to assess fibrosis and cardiomyocyte lipid status. Conduction velocity was significantly greater in epicardial versus endocardial slices in control rats, supporting the concept of a transmural conduction gradient. High-fat diet feeding increased pericardial adiposity and abolished the transmural conduction gradient. Slowed epicardial conduction in epicardial slices strongly correlated with an increase in cardiomyocyte lipid content, but not fibrosis. The positive transmural conduction gradient reported here represents a physiological property of the ventricular activation sequence that likely protects against reentry. The absence of this gradient, secondary to conduction slowing and cardiomyocyte lipid accumulation, specifically in the epicardium, indicates a novel mechanism by which pericardial adiposity may exacerbate ventricular arrhythmias.

Introduction

An organized electrical propagation pathway drives ventricular contraction from the apex to the base, ensuring blood is effectively ejected. Action potentials propagate from the atrioventricular node to the ventricular endocardium via Purkinje fibers and then travel transmurally to the epicardium (Durrer et al., 1970). We and others have shown that endocardial action potential duration is substantially longer than epicardial duration (Wen et al., 2018). This difference serves to offset this transmural delay in activation, synchronizing left ventricular repolarization (Bányász et al., 2003; Boukens et al., 2015; Volk et al., 1999; Wen et al., 2018). Homogenous repolarization prevents functional block, avoiding transmural reentry, and assists in ensuring that the endocardial–epicardial activation sequence is maintained (Boukens et al., 2015). In addition to action potential duration modulation, transmural endocardial–epicardial conduction velocity differences may contribute to determining transmural activation/repolarization patterns. Transmural reentry is an established mechanism implicated in ventricular arrhythmia pathogenesis (Nair et al., 2011; Valderrábano et al., 2001). The underlying early cellular mechanisms that predispose to a transmural reentrant substrate are poorly understood. More specifically, the role of transmural conduction differential in cardiac pathophysiology has not been previously investigated.

Both obesity and a diet rich in saturated fats can increase ventricular arrhythmia vulnerability and are associated with prolonged ventricular repolarization (Omran et al., 2018). This could at least partly be attributed to increased deposition of fibrotic tissue and modification of cross-sarcolemmal channel expression/activity (Powell-Wiley et al., 2021). Pericardial adipose tissue accumulation has also emerged as an important

[1]Department of Anatomy and Physiology, University of Melbourne, Parkville, Australia; [2]Institute of Cardiovascular Sciences, University of Birmingham, Birmingham, UK; [3]Department of Microbiology, Anatomy, Physiology and Pharmacology, La Trobe University, Bundoora, Australia; [4]Department of Physiology, University of Auckland, Auckland, New Zealand; [5]Auckland Bioengineering Institute, University of Auckland, Auckland, New Zealand; [6]Department of Cardiology, Royal Melbourne Hospital, Melbourne, Australia; [7]Department of Medicine, University of Melbourne, Melbourne, Australia; [8]Department of Cardiology, University Heart and Vascular Center Hamburg, University Medical Center Hamburg-Eppendorf, Hamburg, Germany; [9]German Center for Cardiovascular Sciences (DZHK), Partner Site Hamburg-Kiel-Lübeck, Hamburg, Germany.

*L.M.D. Delbridge and J.R. Bell contributed equally to this paper. Correspondence to James R. Bell: j.bell@latrobe.edu.au; Lea M.D. Delbridge: lmd@unimelb.edu.au.

factor determining arrhythmia vulnerability (Ernault et al., 2021). Important in maintaining normal cardiomyocyte fatty acid content under physiological conditions, excessive pericardial adipose tissue can exacerbate fibrosis and disrupt intermyocyte conduction (Nalliah et al., 2020; Venteclef et al., 2015). Much of the work in this field has focused on the link between cardiac adiposity and atrial fibrillation but ventricular adipose deposition has also been identified to correlate with ventricular arrhythmia occurrence (Tam et al., 2016; Wu et al., 2015). An understanding of how ventricular electrophysiology is affected in settings of high cardiac adiposity is severely lacking. The aim of this investigation was therefore to determine whether transmural differences in conduction velocity exist in ventricular tissue and identify to what extent these may be modified in a rat model of pericardial adipose tissue accumulation.

Materials and methods

Animal model

Experiments were conducted in accordance with the Guide for the Care and Use of Laboratory Animals, National Health and Medical Research Council/Commonwealth Scientific, and Industrial Research Organization/ACC Australian Code of Practice for the Care and Use of Animals for Scientific Purposes (1997), as approved (University of Melbourne Animal Ethics Committee). 8-wk-old male Sprague-Dawley rats were fed either a control (Specialty Feeds, SF13-081; 12% lipid energy intake) or high-fat diet (HFD; SF04-001; 43% lipid intake) for 15–16 wk. Food and water were available ad libitum, and intake and body weights were monitored weekly. At the completion of the feeding period, rats were anesthetized with isoflurane and decapitated. Trunk blood was collected for measurement of plasma glucose (ACCU-CHEK Advantage glucometer; Roche Diagnostics) and lipids (cholesterol, triglycerides, and high- and low-density lipoproteins; Cobas B 101; Roche Diagnostics).

Cardiac slice preparation

Tangential left ventricular slices were generated using a modified version of previously published protocols (Fig. 1; Bussek et al., 2009; Watson et al., 2017). Pericardial adipose tissue and hearts were excised and weighed. Hearts were transferred to heparinized ice-cold oxygenated Tyrode's slicing buffer (in mM: NaCl, 140; KCl, 6; glucose, 10; $MgCl_2$, 1; HEPES, 10; $CaCl_2$, 1.8; 2,3-butanedione, 30), the atria resected, and the left ventricular free wall glued epicardial side down onto an agarose-coated specimen holder using Histoacryl surgical glue (B. Braun). This was then transferred into a vibratome bath (7000smz-2; Campden Instruments) containing oxygenated Tyrode's slicing buffer (4°C). 300 µm tangential sections were prepared from the endocardium to the epicardium, cutting along the longitudinal axis of the myocardium using a ceramic blade (0.03 mm/s advance speed, 2 mm amplitude, 80 Hz frequency, <1 µm z-axis error, and ∼8 slices/heart). 300 µm tangential sections have regularly been used in similar preparations, benefitting from the retention of myocardial multicellular composition and capacity for sufficient diffusion of all cells with oxygen and metabolic substrates (Watson et al., 2017). The endocardial slice were defined as the first intact slice generated after trabeculae carneae removal. The epicardial slice was defined as the final intact slice generated.

Microelectrode array recordings and analysis

For electrophysiological mapping, fiber-aligned slices were positioned on a microelectrode array consisting of 60 gold recording electrodes embedded onto a glass substrate in an 8 × 8 matrix (100 µm electrode diameter, 700 µm spacing; 60EcoMEA-Glass-pr; Multichannel Systems). Slices were secured using a custom-made tissue weight and continuously superfused with oxygenated Tyrode's superfusion buffer (37°C, 4 ml/min). Extracellular field potentials were recorded (MEA2100-System; Multichannel Systems) using MC_Rack software (V4.6.2; Multichannel Systems) sampling at 10 KHz (low pass filter: 10 Hz, high pass filter: 3,500 Hz).

Following a 3–5 min equilibration period, slices were paced at the apex of the heart slice along their longitudinal axis using electrodes at the periphery of the tissue at a cycle length of 1,000 ms (biphasic 1 ms pulse for a further 2–3 min). Conduction velocity and field potential duration were then determined from slices paced at a cycle length of 200 ms cycle lengths, consistent with approximate rat physiological pacing in vivo.

All analyses were performed using the final beats of the 200-ms cycle length pacing to allow for sufficient rate adaptation. Analysis of conduction velocity and generation of activation maps was performed using a modified MATLAB-based script (Chowdhury et al., 2018; Watson et al., 2017). Field potential duration was calculated as the interval between the first negative peak on the field potential and the final negative deflection. Local conduction velocity was calculated between neighboring electrodes by dividing the interelectrode distance (700 µm) by the delay in activation. This was calculated between all electrodes and their neighboring counterparts, then an overall mean local conduction velocity value was computed. Longitudinal conduction velocity was calculated by dividing the time delay in activation between the stimulus site and the electrode furthest from that site along the longitudinal axis of the slice (slice fiber orientation was readily distinguishable using a light microscope) by the distance (4.9 mm; i.e., 700 µm interelectrode distance × 7 interelectrode spaces). This was performed for each row along the longitudinal axis, and then the average was calculated. For transverse conduction velocity, the same process was performed, but perpendicular to the longitudinal fiber direction.

Histology

At the end of the electrophysiological mapping protocol, ventricular slices were fixed in 10% formalin (Cat #: HT501128-4L; Sigma-Aldrich) and embedded in optimal cutting temperature (OCT) compound (Cat #: AGR1180; Agar Scientific). Slices were cryosectioned to generate 10 µm sections and stained with either Picrosirius red to identify Collagen Type I and III or Oil Red O to identify neutral lipid droplets (Nalliah et al., 2020).

For imaging of fibrosis, sections were scanned using the brightfield Panoramic SCAN II slide scanner (3DHISTECH) and 10 regions of interest per ventricular slice were captured using CaseViewer (V2.3, 3DHISTECH; 20× magnification). Areas with

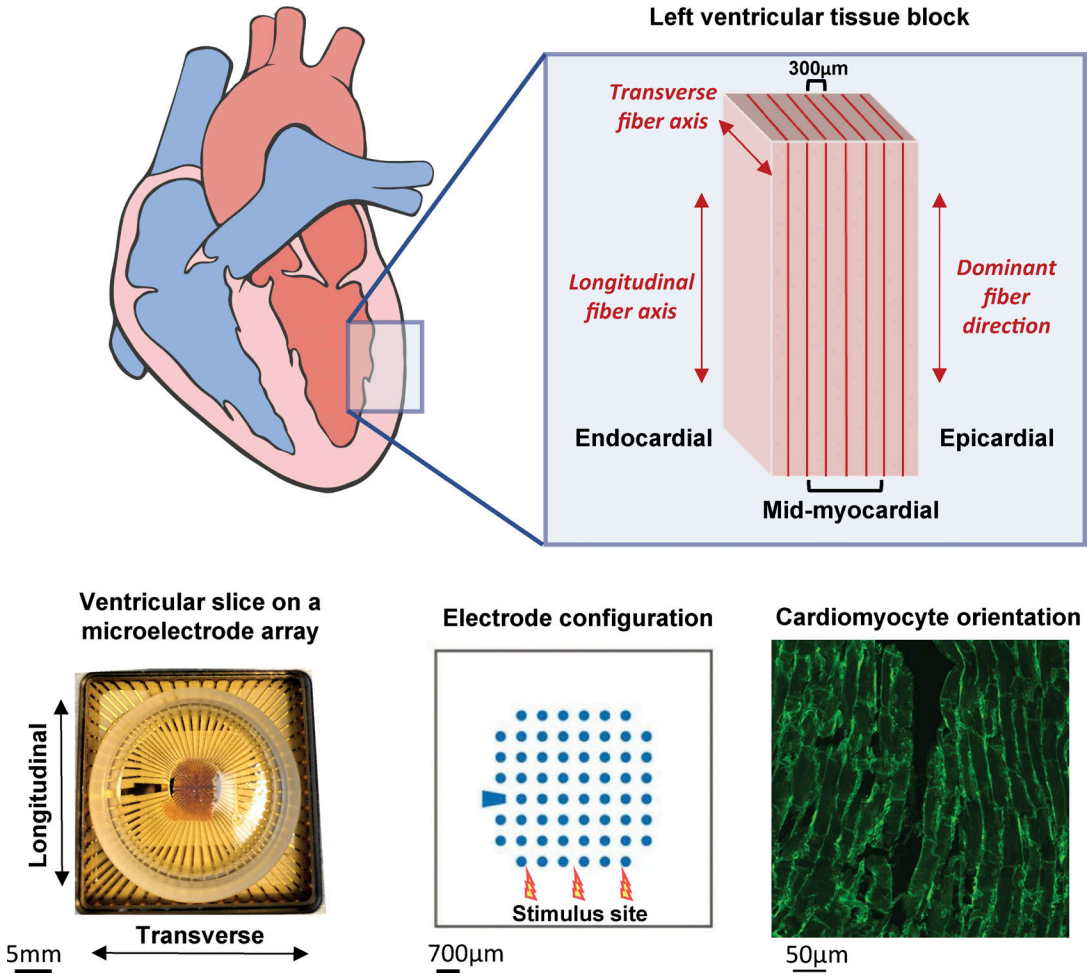

Figure 1. **Generation of tangential left ventricular cardiac slices.** The left ventricular free wall was dissected from freshly isolated rat hearts and sectioned tangentially to generate sequential 300-µm slices. Local field potentials were mapped from electrically paced slices using a microelectrode array. Ventricular slices were positioned to ensure cardiomyocytes were aligned along the longitudinal axis of the microelectrode array.

vascular fibrosis were excluded from the analysis. For neutral lipid droplet detection, images were taken with the brightfield Zeiss Imager D1 microscope, connected to a Zeiss AxioCam MRc5 color camera, and using AxioVision acquisition software (V4.7.1.0; Zeiss; 40× magnification). Image quantification of both fibrosis and neutral lipid droplets was blinded and performed using ImageJ (V1.8). The images were converted to RGB stacks (255 pixel range) and the pixel intensity histogram was used to determine the non-biased threshold to calculate the percent area (% area) as a measure of total fibrosis or total neutral lipid deposition (Curl et al., 2018). For all images, a value of total fibrosis or total lipid deposition was determined and the mean value per animal was calculated.

Statistical analysis

Normally distributed data are presented as mean ± standard error of the mean. Outliers were excluded if >2 standard deviations from the mean and only data with paired endo–epi recordings from a single heart were included. Statistical tests performed are indicated in the figure legends throughout. $P < 0.05$ was deemed significant and n denoted the number of animals/slices used. Statistical analysis of the mean data of two groups was performed using an unpaired t test; effects of HFD and control diet on endo-/epicardial electrophysiological parameters were analyzed by two-way repeated measures ANOVA (diet × endo-/epicardial), with Šidák's multiple comparisons test; correlations between parameters were calculated using a Pearson correlation coefficient (Graph Pad Prism 9).

Results

High-fat feeding leads to pericardial adipose tissue accumulation

15 wk of high-fat feeding had no effect on body weight (control versus HFD: 684.2 ± 21.5 g versus 696.6 ± 34.4 g, P = 0.7746; Fig. 2 A), but a significant increase in pericardial adiposity (311.1 ± 66.0 mg versus 564.8 ± 84.0 mg, P = 0.0410; Fig. 2 B) was observed. The pericardial adipose tissue:body weight was hence markedly elevated in the HFD group (0.45 ± 0.10 mg/g versus 0.79 ± 0.09 mg/g, P = 0.0202; Fig. 2 C). Analysis of the plasma from high-fat and control diet rats showed no difference in glucose (P = 0.8869; Fig. 2 D), cholesterol (P = 0.7893; Fig. 2 E),

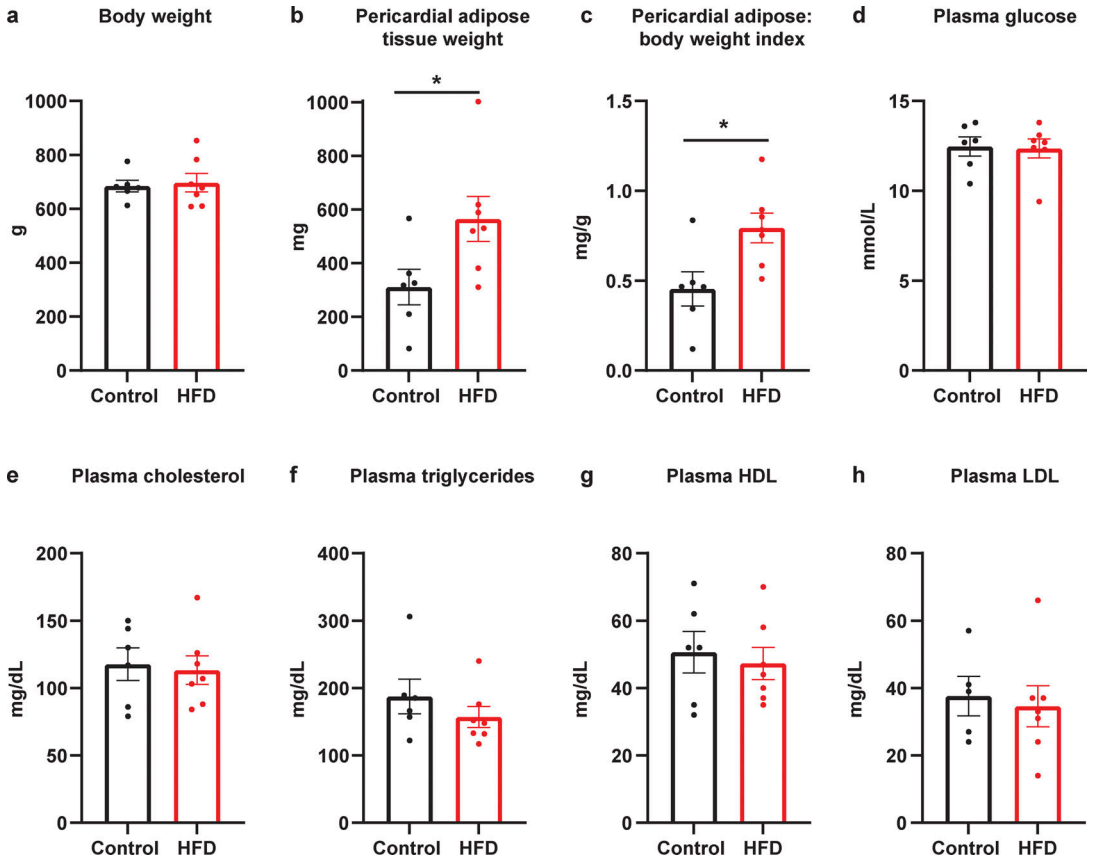

Figure 2. **HFD feeding augmented the extent of pericardial adiposity. (A–H)** Comparison of parameters measured in control and HFD-fed animals include (A) body weight, P = 0.7746; (B) pericardial adipose tissue weight, *P = 0.0410; (C) ratio of pericardial adipose to body weights, *P = 0.0202; (D) plasma glucose, P = 0.8869; (E) plasma cholesterol, P = 0.7893; (F) plasma triglycerides, P = 0.3133; (G) plasma HDL, P = 0.6679; (H) plasma LDL, P = 0.7366. *n* = 6–7 rats. Mean data (±SEM) were presented and analyzed by unpaired *t* tests.

triglyceride (P = 0.3133; Fig. 2 F), high-density lipoprotein (HDL; P = 0.6679; Fig. 2 G), or low-density lipoprotein (LDL; P = 0.7366; Fig. 2 H) levels.

High-fat feeding abolishes the transmural conduction gradient

Control and HFD-fed rat tissues demonstrated similar endocardial and epicardial field potential durations—both with clear transmural differences (Fig. 3, A–C). This contrasted with conduction velocity observations along the longitudinal axes of the endo-/epicardial slices (Fig. 3, D–F). Endocardial tissue slices of control and HFD rats exhibited similar conduction velocities (Fig. 3, D and E). The marked endo-/epicardial increase in conduction velocity evident in tissue slices of control animals was not observed in the HFD-derived slices (Fig. 3 F). This was primarily attributed to slowed epicardial conduction velocity in HFD rats, abrogating the transmural conduction velocity gradient (Δendocardial–epicardial conduction velocity, control versus HFD: 20.7 ± 3.6 cm/s versus 3.3 ± 3.5 cm/s, P = 0.0045; Fig. 3 F).

Slowed epicardial conduction velocity strongly correlates with cardiomyocyte lipid accumulation

Endocardial and epicardial slices were cryosectioned and stained with Picrosirius red to quantify fibrosis (Fig. 4 A). In control rat ventricles, the extent of fibrosis did not differ between endocardial and epicardial sections (Fig. 4 B). High-fat feeding was associated with greater fibrosis in endocardial (versus control) but not epicardial sections (versus control; Fig. 4 B).

To assess whether high-fat feeding modulates cellular lipid content, sections were stained with Oil Red O (Fig. 4 C). No difference in cardiomyocyte lipid content was evident in endocardial and epicardial sections from control rat ventricles. High-fat feeding significantly increased cardiomyocyte lipid content (versus control) and was significantly greater in epicardial compared with endocardial sections (Fig. 4 D).

The electrophysiological implications of these changes in fibrosis and cardiomyocyte lipid content were then assessed (Fig. 5, A–D). No correlation was evident between the extent of fibrosis and conduction velocity in either endocardial or epicardial sections (Fig. 5, A and B). In contrast, a strong correlation was observed between cardiomyocyte lipid content and conduction velocity in epicardial sections, with cardiomyocyte lipid accumulation associated with slowed conduction (Fig. 5 D). This relationship was not evident in endocardial sections (Fig. 5 C).

Discussion

This study demonstrates an increase in conduction velocity in epicardial ventricular slices relative to endocardial slices. This is

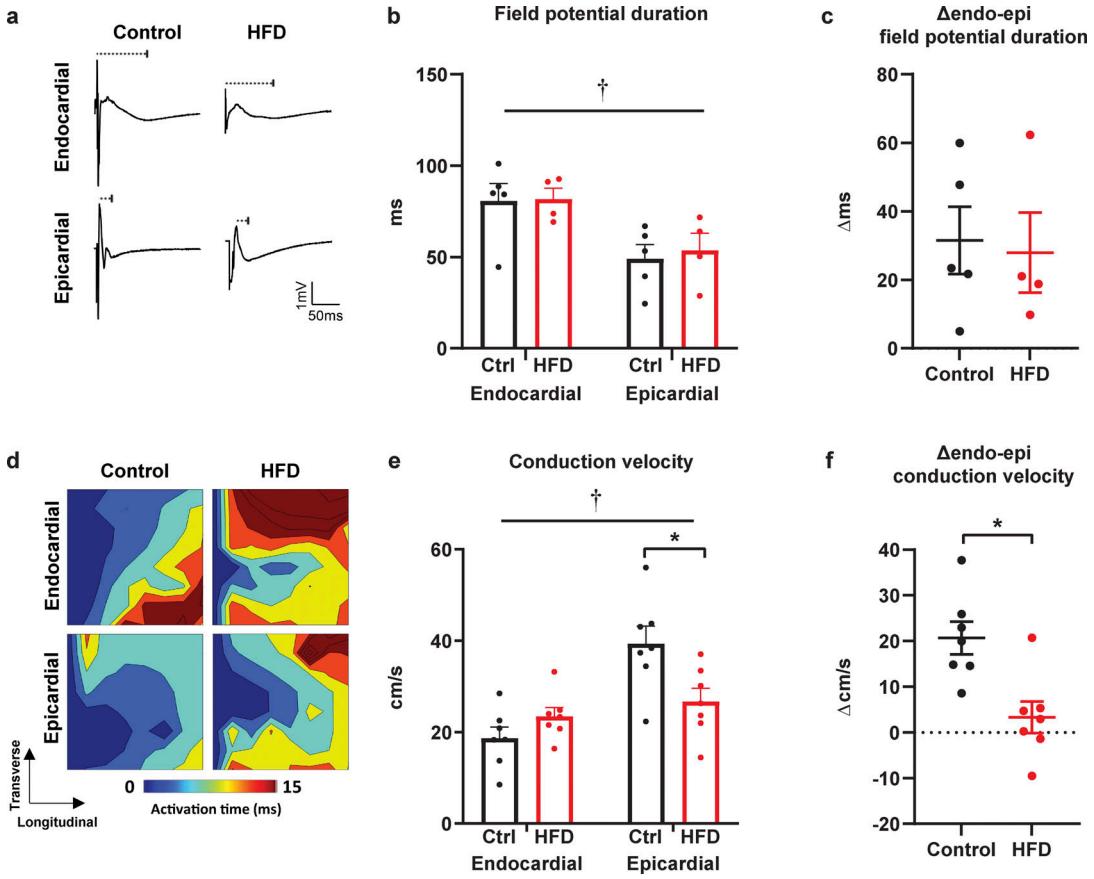

Figure 3. **Ventricular transmural conduction gradient is absent in HFD-fed rat hearts. (A)** Exemplar endocardial and epicardial field potentials from control (ctrl) and HFD rats. **(B)** Mean field potential duration in endocardial and epicardial slices from control and HFD fed rats; †P = 0.0164 for transmural region effect. **(C)** Mean change in field potential duration in endocardial and epicardial slices from each heart, P = 0.6278 for diet effect. **(D)** Exemplar activation maps from endocardial and epicardial ventricular slices in control and HFD rats (3 ms isochrones shown). **(E)** Mean conduction velocity in endocardial and epicardial slices from control and HFD fed rats, †P = 0.0004 for transmural region effect, *P = 0.0094 for diet effect. **(F)** Mean change in conduction velocity in endocardial and epicardial slices from each heart; *P = 0.0045 for diet effect. *n* = 4–7 slices. Mean data (±SEM) presented. Effects of HFD and control diet on endo-/epicardial electrophysiological parameters analyzed by two-way repeated measures ANOVA, with Šidák's multiple comparisons test; comparison of the change in electrophysiological parameters in HFD versus control diet analyzed by unpaired *t* tests.

indicative of a transmural conduction gradient within the myocardium that is predicted to contribute to coordinated ventricular transmural activation/repolarization in physiological settings. Following a high-fat dietary intervention, pericardial adipose accumulates and the transmural conduction gradient diminishes. This degree of epicardial conduction slowing was related to the cardiomyocyte lipid content. These findings suggest a potentially important association between cardiomyocyte fat incorporation and ventricular conduction properties, which may provide a novel mechanism linking ventricular arrhythmias to a HFD, pericardial adipose accumulation, and obesity.

Physiological role of transmural differences in ventricular conduction velocity

Ventricular slices from control rats demonstrated a clear transmural difference in field potential duration, with field potential prolongation evident in epicardial sections compared with endocardial. This transmural difference has been established in various species/preparations, though we believe this is the first demonstration in transmurally uncoupled tissue slices (Bányász et al., 2003; Boukens et al., 2015; Volk et al., 1999; Wen et al., 2018). The transmural repolarization gradient is required for normal electromechanical function of the ventricle (Opthof et al., 2016) and reduces reentrant arrhythmia vulnerability. We also showed evidence of an accompanying transmural gradient in conduction velocity, with epicardial conduction significantly faster than endocardial. This transmural conduction velocity gradient may also exert an important physiological role in the heart. As the myocardium activates from the endocardium to the epicardium, such a conduction velocity gradient would be expected to confer a delay between endocardial and epicardial depolarization (Durrer et al., 1970). The more rapid action potential propagation rate at the epicardium would be predicted to allow completion of an epicardial activation cycle before the endocardium becomes reexcitable, synchronizing transmural repolarization and hence reducing the potential for transmural reentry.

Pericardial adipose accumulation in HFD-fed rats

To assess the effect of a HFD on transmural conduction properties, rats were fed a HFD, corresponding to a 43% energy

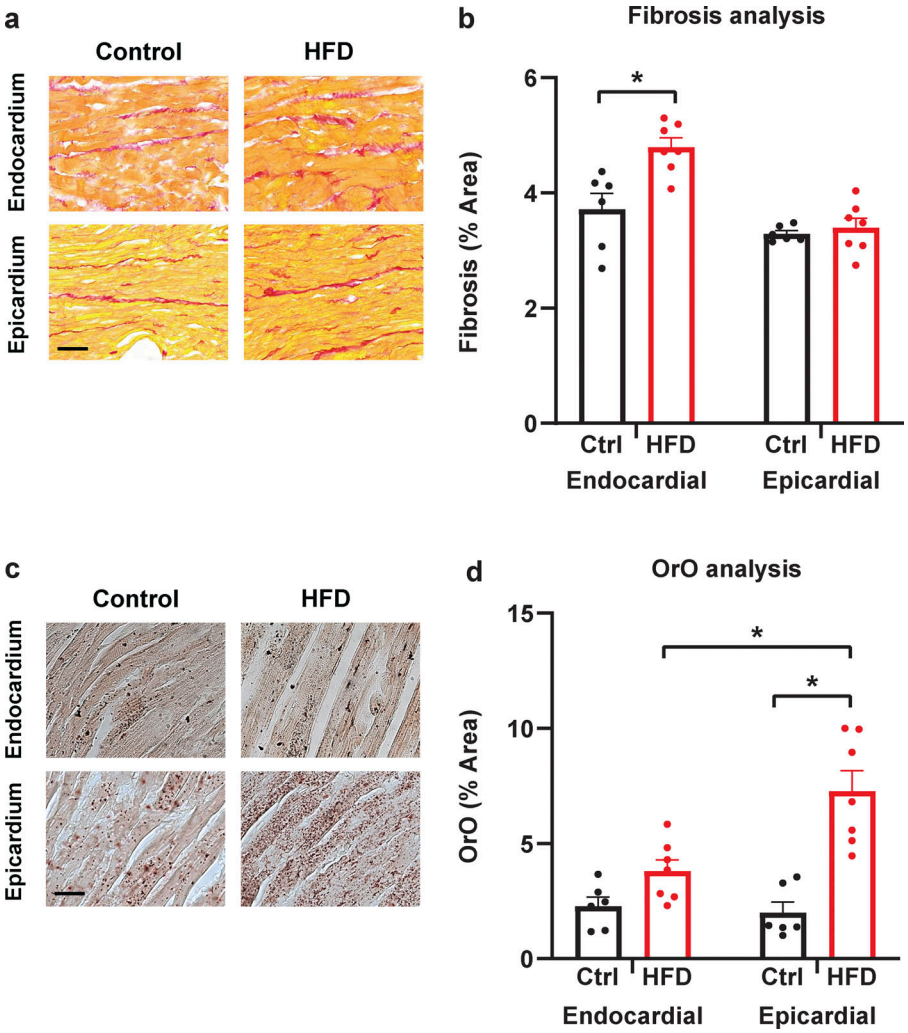

Figure 4. **HFD feeding is associated with greater cardiomyocyte lipid accumulation.** **(A)** Exemplar endocardial and epicardial sections stained with picrosirius red for evaluation of the extent of fibrosis. **(B)** Mean fibrosis in endocardial and epicardial sections from control (ctrl) and HFD rats; *P = 0.0022 HFD versus control in endocardial slices. **(C)** Exemplar endocardial and epicardial sections stained with Oil Red O for quantification of cellular lipid accumulation. **(D)** Mean cellular lipid content in endocardial and epicardial sections from control and HFD rats; *P = 0.0025 endocardial versus endocardial in HFD slices. *n* = 6–7 sections. Mean data (±SEM) presented. Effects of HFD and control diet on endo-/epicardial histology analyzed by two-way repeated measures ANOVA, with Šidák's multiple comparisons test.

intake from lipids. Though rat body weight did not change (versus control diet), a significant increase in pericardial adipose tissue weight was observed (Fig. 2). Considering the relatively low abundance of adipose on the epicardial surface of rodent hearts compared with larger animals (Suffee et al., 2017), the accumulation of pericardial adipose reported refers to the paracardial depot—the adipose in direct contact with the pericardium. In rodents, the pericardium exhibits numerous pores, allowing direct exposure of the myocardium to paracrine mediators released from this adipose depot (Bale et al., 2018; Nakatani et al., 1988).

The absence of an increase in body weight may be explained by the accumulating evidence of diet- and species/strain-specific responses to HFD feeding. Many rodent obesity models utilize HFDs with >60% energy intake from lipids. This benefits from its capacity to accelerate and augment general adiposity gain, but may not accurately model the human condition. The fat content of the diet in our study (43% energy intake from lipids) is more consistent with that of a typical "Western" diet (Speakman, 2019). Additionally, Sprague-Dawley rats have been reported to be more resistant to body weight gain in settings of HFD feeding compared with other rat strains (Marques et al., 2015). Considering no change in plasma glucose and lipids in the absence of increased body or heart weight gain, this model may selectively provide important insights into the possible influence of pericardial adiposity on cardiac electrophysiology and highlight that increased cardiac adiposity may precede general body adiposity to initiate the demise of the heart.

Dissipation of the ventricular transmural conduction velocity gradient

To understand the extent to which this transmural conduction velocity gradient may change in a pathological setting, further studies were conducted with ventricular slices sourced from rats fed a HFD. Obesity and a diet rich in saturated fats are clinical risk factors for arrhythmias and are associated with changes in the electrophysiological properties of the heart. HFD feeding led to a loss of the transmural conduction velocity gradient across the ventricular slices—specifically due to a relative slowing of the epicardial conduction velocity to levels similar to those observed in the endocardial slices (Fig. 3, E and F). Slowed conduction velocity is an important mechanism underlying the establishment of reentrant arrhythmias (Han et al., 2021). This can occur intramurally (i.e., within the epicardium) or transmurally in a retrograde direction due to the regional effect of the conduction slowing. We and others have shown that greater

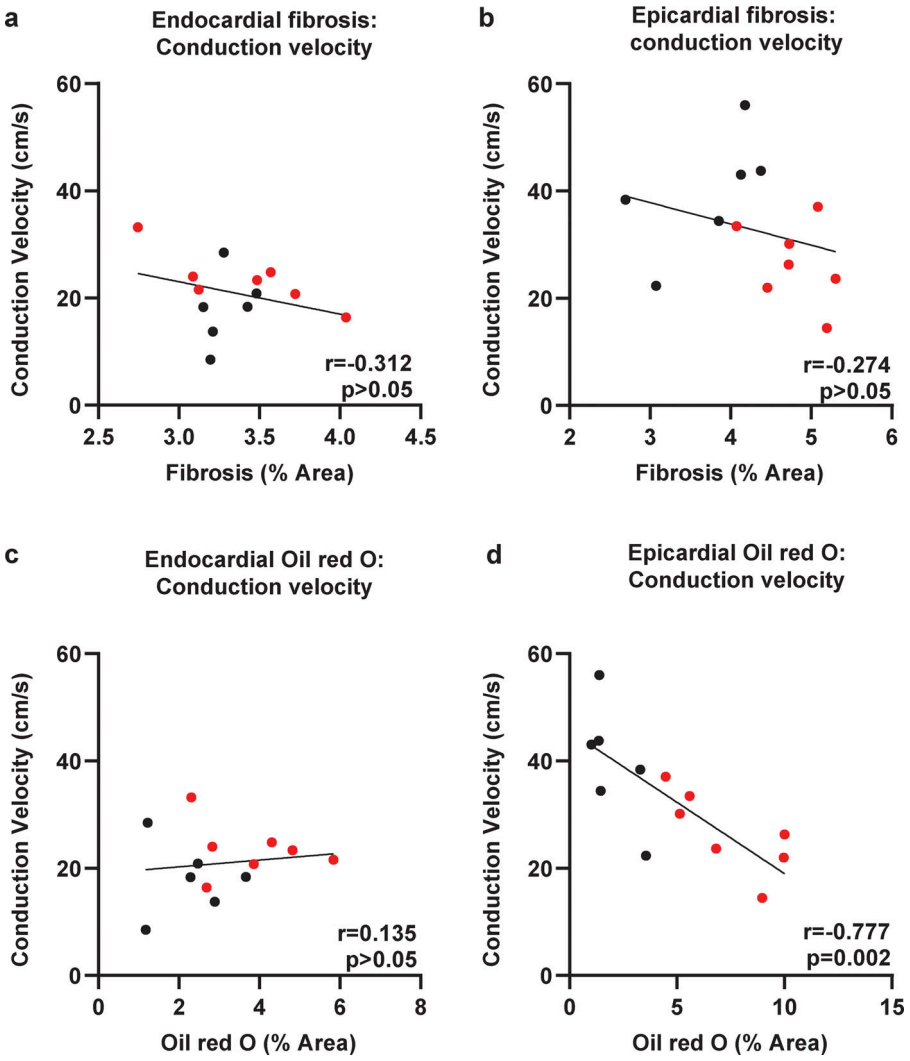

Figure 5. **Epicardial, but not endocardial, conduction velocity strongly correlates with cardiomyocyte lipid content. (A and B)** Correlation analysis of conduction velocity and fibrosis in ventricular endocardial (P = 0.299) and epicardial (P = 0.366) slices from the control (black dots) and HFD-fed (red dots) rat hearts. **(C and D)** Correlation analysis of conduction velocity and cellular lipid content in ventricular endocardial (P = 0.659) and epicardial (P = 0.002) slices. *n* = 6–7 sections. Correlations between parameters were calculated using a Pearson correlation coefficient.

pericardial adiposity can lead to localized conduction slowing (Mahajan et al., 2015; Nalliah et al., 2020). This has previously been attributed to adipose tissue infiltration of the myocardium and associated ventricular fibrosis (Mahajan et al., 2015; Nalliah et al., 2020; Venteclef et al., 2015), instigating localized physical disruption of intermyocyte connectivity and regionalized conduction slowing. We more recently identified a novel pericardial adipose–cardiomyocyte paracrine axis that also slows intermyocyte conduction and contributes to the conduction heterogeneities associated with cardiac adiposity (Nalliah et al., 2020).

Figs. 4 and 5 indicate that fibrosis does not contribute to the relative decrease in epicardial conduction velocity and loss of transmural gradient. Indeed, fibrosis was greater only in the endocardial slices from HFD-fed hearts, and no correlation was observed between conduction velocity and fibrosis in endocardial or epicardial slices. Rather, a strong link between epicardial conduction slowing and the extent of cardiomyocyte lipid accumulation was observed. HFD is linked with increased cardiomyocyte lipid content, indicating an inability to properly regulate cellular fatty acid uptake and/or utilization (Axelsen et al., 2015; Christoffersen et al., 2003; Sharma et al., 2004; Szczepaniak et al., 2007). This is associated with decreased Cx43 protein expression and an apparent lateral positioning within the cardiomyocyte, both of which likely contribute to the reported ventricular conduction slowing and arrhythmia vulnerability (Axelsen et al., 2015; Joseph et al., 2019; Lin et al., 2005; Takahashi et al., 2016). Similar phenotypic characteristics have also been reported in transgenic peroxisome proliferated activated receptor γ1 (PPARγ1) overexpression model of cardiomyocyte lipid accumulation (Morrow et al., 2011).

Our data is novel in that we show the existence of a transmural gradient of cardiomyocyte lipid accumulation, and with it a loss of the transmural conduction velocity gradient. This being evident in a model of high pericardial adiposity is intriguing and suggests the myocardium in closest proximity to the adipose tissue is unable to sufficiently manage the cardiomyocyte fatty acid load. It is neither clear how this occurs nor the mechanism by which localized cardiomyocyte lipid accumulation may contribute to conduction slowing. This is likely multifactorial, involving changes in cellular metabolism, redox status, and lipid-mediated protein modification that culminate in the activation of intracellular signaling cascades regulating ion channel function and intermyocyte connectivity (Axelsen et al., 2015; Joseph et al., 2019; Lin et al., 2005; Morrow et al., 2011; Szczepaniak et al.,

2007; Takahashi et al., 2016). Lipids play an important role in the regulation of ion channel function, either through direct modulation of channel structure or changes to the surrounding lipid bilayer. Actions on channel activity are dependent on lipid type; generally, there is a propensity for cholesterol to inhibit inwardly rectifying K^+, voltage-gated K^+, Na^+, and Ca^{2+} channels contrasting with the stimulatory influence of phosphatidylinositol 4,5-bisphosphate (PIP2; Rosenhouse-Dantsker et al., 2012). The extent to which cardiomyocyte lipid accumulation affects channel activity and/or expression in epicardial slices from HFD-fed rat hearts is unclear. Further studies are required to interrogate candidate processes within the cardiomyocyte that may be responsible and how lipid accumulation may underlie the absence of transmural conduction gradients in a setting of HFD feeding.

Study limitations

Previous studies have utilized numerous different in vivo, ex vivo, and in vitro models/methodologies to assess transmural electrophysiological gradients. In the current study, transmurally uncoupled tissue slices were used to assess the impact HFD feeding has on these conduction gradients. 300-µm tangential slices in this study have regularly been used in similar preparations (Watson et al., 2017). These highly viable preparations are thin enough to facilitate sufficient diffusion of all cells with oxygen and metabolic substrates whilst retaining the multicellular composition of the myocardium (Nerlekar et al., 2018). By slicing along the longitudinal axis of the heart parallel to endo-/epicardial fiber orientation, damage to the myocardial fibers within each slice has been minimized.

We acknowledge that Purkinje fibers within the endocardial slices would likely influence both the anisotropic properties and mean conduction velocity across slices. In the current study, an initial slice was performed to remove the trabeculae carnae to optimize myocardial contact across all microelectrode array electrodes. The extent to which Purkinje fibers are present in the endocardial slices assessed is therefore unclear. Additionally, the use of ventricular slices on a multielectrode array allows only for the assessment of conduction properties along the 2-D plane of contact between the slice and array surface. We predict there may be up to 20 layers of cardiomyocytes across the depth of each 300 µm slice (Satoh et al., 1996), of which it would be predicted that variabilities in cardiomyocyte alignment in both the longitudinal and transverse dimensions exist. Interpretation of the results presented here should hence factor in the limitations associated with the presence of Purkinje fibers and transmural anisotropic variations within each slice. Nevertheless, our findings of slower conduction in endocardial versus epicardial myocardium in the control-fed rats are consistent with the literature and do not detract from the novel findings of a relative slowing of conduction in the epicardial slices from HFD-fed rats. Additional studies using either perfused wedge preparations or Langendorff hearts could be used to confirm these findings and provide additional insights in relation to the limitations highlighted.

Conclusions

We have shown that a positive transmural conduction gradient is absent in settings of high-fat feeding. We predict that this could lead to the desynchronization of transmural repolarization which may increase the potential for transmural reentry. This is consistent with the greater arrhythmia vulnerability previously reported with high-fat feeding. This may be linked to an increase in cardiac adiposity, which has emerged as a marker for arrhythmia risk. To date, the field has almost entirely focused on the development of atrial fibrillation, yet epidemiological data supports an association between pericardial adipose tissue deposition and ventricular fibrillation/sudden cardiac death (Nerlekar et al., 2018; Lee et al., 2011; Wu et al., 2015; Sepehri Shamloo et al., 2019). Our data now indicate that the accumulation of cardiomyocyte lipid droplets in a setting of pericardial adiposity is also likely involved, thereby providing a novel, direct proarrhythmic effect of a HFD.

Data availability

The datasets generated and analyzed during this study are included in this article. The raw data are available from the corresponding authors upon reasonable request.

Acknowledgments

Jeanne M. Nerbonne served as editor.

MATLAB script for the generation of activation maps and conduction velocity analysis was kindly provided by Professor Cesare Terracciano, Imperial College London (London, UK), and is gratefully acknowledged. Technical support was provided by the Melbourne Histology Platform.

This research was supported by the National Health and Medical Research Council (grants #1099352 and #1125453; to L.M.D. Delbridge and J.R. Bell) and the Australian Research Council (grant #DP160102404; to L.M.D. Delbridge). D. Pavlovic is supported by the British Heart Foundation (PG/17/55/33087; RG/17/15/33106; FS/19/12/34204; FS/19/16/34169). C. O'Shea is supported by a Sir Henry Wellcome Fellowship, Wellcome Trust, 221650/Z/20/Z.

Author contributions: S.P. Wells, D. Pavlovic, L.M.D. Delbridge, and J.R. Bell designed the research; S.P. Wells, A.J.A. Raaijmakers, S. Hayes, and J.R. Bell performed experiments; S.P. Wells, A.J.A. Raaijmakers, C.L. Curl, C. O'Shea, S. Hayes, and J.R. Bell analyzed data; and S.P. Wells, K.M. Mellor, J.M. Kalman, L.M.D. Delbridge, and J.R. Bell wrote the paper. All authors approved the final version of the manuscript.

Disclosures: J.M. Kalman reported grants from Medtronic Inc., Biosense Webster, and Zoll outside the submitted work; and Practitioner Fellowship, National Health and Medical Research Council of Australia. P. Kirchhof reported grants from DZHK, BHF, and EU during the conduct of the study, and grants from several companies active in atrial fibrillation outside the submitted work; in addition, P. Kirchhof had a patent to two patents owned by UKE granted issued. No other disclosures were reported.

Submitted: 16 November 2022
Revised: 20 May 2023
Accepted: 29 August 2023

References

Axelsen, L.N., K. Calloe, T.H. Braunstein, M. Riemann, J.P. Hofgaard, B. Liang, C.F. Jensen, K.B. Olsen, E.D. Bartels, U. Baandrup, et al. 2015. Diet-induced pre-diabetes slows cardiac conductance and promotes arrhythmogenesis. *Cardiovasc. Diabetol.* 14:87. https://doi.org/10.1186/s12933-015-0246-8

Bale, L.K., S.A. West, and C.A. Conover. 2018. Characterization of mouse pericardial fat: Regulation by PAPP-A. *Growth Horm. IGF Res.* 42-43:1–7. https://doi.org/10.1016/j.ghir.2018.07.002

Bányász, T., L. Fülöp, J. Magyar, N. Szentandrássy, A. Varró, and P.P. Nánási. 2003. Endocardial versus epicardial differences in L-type calcium current in canine ventricular myocytes studied by action potential voltage clamp. *Cardiovasc. Res.* 58:66–75. https://doi.org/10.1016/S0008-6363(02)00853-2

Boukens, B.J., M.S. Sulkin, C.R. Gloschat, F.S. Ng, E.J. Vigmond, and I.R. Efimov. 2015. Transmural APD gradient synchronizes repolarization in the human left ventricular wall. *Cardiovasc. Res.* 108:188–196. https://doi.org/10.1093/cvr/cvv202

Bussek, A., E. Wettwer, T. Christ, H. Lohmann, P. Camelliti, and U. Ravens. 2009. Tissue slices from adult mammalian hearts as a model for pharmacological drug testing. *Cell. Physiol. Biochem.* 24:527–536. https://doi.org/10.1159/000257528

Chowdhury, R.A., K.N. Tzortzis, E. Dupont, S. Selvadurai, F. Perbellini, C.D. Cantwell, F.S. Ng, A.R. Simon, C.M. Terracciano, and N.S. Peters. 2018. Concurrent micro- to macro-cardiac electrophysiology in myocyte cultures and human heart slices. *Sci. Rep.* 8:6947. https://doi.org/10.1038/s41598-018-25170-9

Christoffersen, C., E. Bollano, M.L. Lindegaard, E.D. Bartels, J.P. Goetze, C.B. Andersen, and L.B. Nielsen. 2003. Cardiac lipid accumulation associated with diastolic dysfunction in obese mice. *Endocrinology*. 144:3483–3490. https://doi.org/10.1210/en.2003-0242

Curl, C.L., V.R. Danes, J.R. Bell, A.J.A. Raaijmakers, W.T.K. Ip, C. Chandramouli, T.W. Harding, E.R. Porrello, J.R. Erickson, F.J. Charchar, et al. 2018. Cardiomyocyte functional etiology in heart failure with preserved ejection fraction is distinctive-A new preclinical model. *J. Am. Heart Assoc.* 7:e007451. https://doi.org/10.1161/JAHA.117.007451

Durrer, D., R.T. van Dam, G.E. Freud, M.J. Janse, F.L. Meijler, and R.C. Arzbaecher. 1970. Total excitation of the isolated human heart. *Circulation*. 41:899–912. https://doi.org/10.1161/01.CIR.41.6.899

Ernault, A.C., V.M.F. Meijborg, and R. Coronel. 2021. Modulation of cardiac arrhythmogenesis by epicardial adipose tissue: JACC State-of-the-Art Review. *J. Am. Coll. Cardiol.* 78:1730–1745. https://doi.org/10.1016/j.jacc.2021.08.037

Han, B., M.L. Trew, and C.M. Zgierski-Johnston. 2021. Cardiac conduction velocity, remodeling and arrhythmogenesis. *Cells*. 10:2923. https://doi.org/10.3390/cells10112923

Joseph, L.C., U.M.R. Avula, E.Y. Wan, M.V. Reyes, K.R. Lakkadi, P. Subramanyam, K. Nakanishi, S. Homma, A. Muchir, U.B. Pajvani, et al. 2019. Dietary saturated fat promotes arrhythmia by activating NOX2 (NADPH oxidase 2). *Circ. Arrhythm. Electrophysiol.* 12:e007573. https://doi.org/10.1161/CIRCEP.119.007573

Lee, D.S., P. Gona, I. Albano, M.G. Larson, E.J. Benjamin, D. Levy, W.B. Kannel, and R.S. Vasan. 2011. A systematic assessment of causes of death after heart failure onset in the community: Impact of age at death, time period, and left ventricular systolic dysfunction. *Circ. Heart Fail.* 4:36–43. https://doi.org/10.1161/CIRCHEARTFAILURE.110.957480

Lin, L.C., C.C. Wu, H.I. Yeh, L.S. Lu, Y.B. Liu, S.F. Lin, and Y.T. Lee. 2005. Downregulated myocardial connexin 43 and suppressed contractility in rabbits subjected to a cholesterol-enriched diet. *Lab. Invest.* 85:1224–1237. https://doi.org/10.1038/labinvest.3700324

Mahajan, R., D.H. Lau, A.G. Brooks, N.J. Shipp, J. Manavis, J.P. Wood, J.W. Finnie, C.S. Samuel, S.G. Royce, D.J. Twomey, et al. 2015. Electrophysiological, electroanatomical, and structural remodeling of the atria as consequences of sustained obesity. *J. Am. Coll. Cardiol.* 66:1–11. https://doi.org/10.1016/j.jacc.2015.04.058

Marques, C., M. Meireles, S. Norberto, J. Leite, J. Freitas, D. Pestana, A. Faria, and C. Calhau. 2015. High-fat diet-induced obesity rat model: A comparison between wistar and sprague-dawley rat. *Adipocyte*. 5:11–21. https://doi.org/10.1080/21623945.2015.1061723

Morrow, J.P., A. Katchman, N.H. Son, C.M. Trent, R. Khan, T. Shiomi, H. Huang, V. Amin, J.M. Lader, C. Vasquez, et al. 2011. Mice with cardiac overexpression of peroxisome proliferator-activated receptor γ have impaired repolarization and spontaneous fatal ventricular arrhythmias. *Circulation*. 124:2812–2821. https://doi.org/10.1161/CIRCULATIONAHA.111.056309

Nair, K., K. Umapathy, T. Farid, S. Masse, E. Mueller, R.V. Sivanandan, K. Poku, V. Rao, V. Nair, J. Butany, et al. 2011. Intramural activation during early human ventricular fibrillation. *Circ. Arrhythm. Electrophysiol.* 4:692–703. https://doi.org/10.1161/CIRCEP.110.961037

Nakatani, T., H. Shinohara, Y. Fukuo, S. Morisawa, and T. Matsuda. 1988. Pericardium of rodents: Pores connect the pericardial and pleural cavities. *Anat. Rec.* 220:132–137. https://doi.org/10.1002/ar.1092200204

Nalliah, C.J., J.R. Bell, A.J.A. Raaijmakers, H.M. Waddell, S.P. Wells, G.B. Bernasochi, M.K. Montgomery, S. Binny, T. Watts, S.B. Joshi, et al. 2020. Epicardial adipose tissue accumulation confers atrial conduction abnormality. *J. Am. Coll. Cardiol.* 76:1197–1211. https://doi.org/10.1016/j.jacc.2020.07.017

Nerlekar, N., R.G. Muthalaly, N. Wong, U. Thakur, D.T.L. Wong, A.J. Brown, and T.H. Marwick. 2018. Association of volumetric epicardial adipose tissue quantification and cardiac structure and function. *J. Am. Heart Assoc.* 7:e009975. https://doi.org/10.1161/JAHA.118.009975

Omran, J., B.P. Bostick, A.K. Chan, and M.A. Alpert. 2018. Obesity and ventricular repolarization: A comprehensive review. *Prog. Cardiovasc. Dis.* 61:124–135. https://doi.org/10.1016/j.pcad.2018.04.004

Opthof, T., M.J. Janse, V.M. Meijborg, J. Cinca, M.R. Rosen, and R. Coronel. 2016. Dispersion in ventricular repolarization in the human, canine and porcine heart. *Prog. Biophys. Mol. Biol.* 120:222–235. https://doi.org/10.1016/j.pbiomolbio.2016.01.007

Powell-Wiley, T.M., P. Poirier, L.E. Burke, J.P. Després, P. Gordon-Larsen, C.J. Lavie, S.A. Lear, C.E. Ndumele, I.J. Neeland, P. Sanders, and M.P. St-Onge. 2021. Obesity and cardiovascular disease: A scientific statement from the American heart association. *Circulation*. 143:e984–e1010. https://doi.org/10.1161/CIR.0000000000000973

Rosenhouse-Dantsker, A., D. Mehta, and I. Levitan. 2012. Regulation of ion channels by membrane lipids. *Compr. Physiol.* 2:31–68. https://doi.org/10.1002/cphy.c110001

Satoh, H., L.M. Delbridge, L.A. Blatter, and D.M. Bers. 1996. Surface:volume relationship in cardiac myocytes studied with confocal microscopy and membrane capacitance measurements: Species-dependence and developmental effects. *Biophys. J.* 70:1494–1504. https://doi.org/10.1016/S0006-3495(96)79711-4

Sepehri Shamloo, A., K. Schoene, A. Stauber, A. Darma, N. Dagres, B. Dinov, L. Bertagnolli, S. Hilbert, A. Müssigbrodt, D. Husser, et al. 2019. Epicardial adipose tissue thickness as an independent predictor of ventricular tachycardia recurrence following ablation. *Heart Rhythm*. 16:1492–1498. https://doi.org/10.1016/j.hrthm.2019.06.009

Sharma, S., J.V. Adrogue, L. Golfman, I. Uray, J. Lemm, K. Youker, G.P. Noon, O.H. Frazier, and H. Taegtmeyer. 2004. Intramyocardial lipid accumulation in the failing human heart resembles the lipotoxic rat heart. *FASEB J.* 18:1692–1700. https://doi.org/10.1096/fj.04-2263com

Speakman, J.R. 2019. Use of high-fat diets to study rodent obesity as a model of human obesity. *Int. J. Obes.* 43:1491–1492. https://doi.org/10.1038/s41366-019-0363-7

Suffee, N., T. Moore-Morris, P. Farahmand, C. Rücker-Martin, G. Dilanian, M. Fradet, D. Sawaki, G. Derumeaux, P. LePrince, K. Clément, et al. 2017. Atrial natriuretic peptide regulates adipose tissue accumulation in adult atria. *Proc. Natl. Acad. Sci. USA*. 114:E771–E780. https://doi.org/10.1073/pnas.1610968114

Szczepaniak, L.S., R.G. Victor, L. Orci, and R.H. Unger. 2007. Forgotten but not gone: The rediscovery of fatty heart, the most common unrecognized disease in America. *Circ. Res.* 101:759–767. https://doi.org/10.1161/CIRCRESAHA.107.160457

Takahashi, K., T. Sasano, K. Sugiyama, J. Kurokawa, N. Tamura, Y. Soejima, M. Sawabe, M. Isobe, and T. Furukawa. 2016. High-fat diet increases vulnerability to atrial arrhythmia by conduction disturbance via miR-27b. *J. Mol. Cell. Cardiol.* 90:38–46. https://doi.org/10.1016/j.yjmcc.2015.11.034

Tam, W.C., Y.K. Lin, W.P. Chan, J.H. Huang, M.H. Hsieh, S.A. Chen, and Y.J. Chen. 2016. Pericardial fat is associated with the risk of ventricular arrhythmia in asian patients. *Circ. J.* 80:1726–1733. https://doi.org/10.1253/circj.CJ-16-0047

Valderrábano, M., M.-H. Lee, T. Ohara, A.C. Lai, M.C. Fishbein, S.-F. Lin, H.S. Karagueuzian, and P.-S. Chen. 2001. Dynamics of intramural and transmural reentry during ventricular fibrillation in isolated swine ventricles. *Circ. Res.* 88:839–848. https://doi.org/10.1161/hh0801.089259

Venteclef, N., V. Guglielmi, E. Balse, B. Gaborit, A. Cotillard, F. Atassi, J. Amour, P. Leprince, A. Dutour, K. Clément, and S.N. Hatem. 2015. Human epicardial adipose tissue induces fibrosis of the atrial

myocardium through the secretion of adipo-fibrokines. *Eur. Heart J.* 36: 795–805a. https://doi.org/10.1093/eurheartj/eht099

Volk, T., T.H. Nguyen, J.H. Schultz, and H. Ehmke. 1999. Relationship between transient outward K+ current and Ca2+ influx in rat cardiac myocytes of endo- and epicardial origin. *J. Physiol.* 519:841–850. https://doi.org/10.1111/j.1469-7793.1999.0841n.x

Watson, S.A., M. Scigliano, I. Bardi, R. Ascione, C.M. Terracciano, and F. Perbellini. 2017. Preparation of viable adult ventricular myocardial slices from large and small mammals. *Nat. Protoc.* 12:2623–2639. https://doi.org/10.1038/nprot.2017.139

Wen, Q., K. Gandhi, R.A. Capel, G. Hao, C. O'Shea, G. Neagu, S. Pearcey, D. Pavlovic, D.A. Terrar, J. Wu, et al. 2018. Transverse cardiac slicing and optical imaging for analysis of transmural gradients in membrane potential and Ca^{2+} transients in murine heart. *J. Physiol.* 596:3951–3965. https://doi.org/10.1113/JP276239

Wu, C.K., H.Y. Tsai, M.Y. Su, Y.F. Wu, J.J. Hwang, W.Y. Tseng, J.L. Lin, and L.Y. Lin. 2015. Pericardial fat is associated with ventricular tachyarrhythmia and mortality in patients with systolic heart failure. *Atherosclerosis*. 241:607–614. https://doi.org/10.1016/j.atherosclerosis.2015.05.025